Electrolyte distribution and discharge time – a combined study of X-ray tomography and electrical measurements of a commercially available lithium-ion capacitor

F. Wieder (a), Ch. Kallfaß (b), I. Manke (c), A. Hilger (c), C. Tötzke (a, c), C. Hoch (d),
H. Schier (e), K. Graf (e) and J. Banhart (a, c)

(a) Technische Universität Berlin, 10623 Berlin, Germany
(b) Goodrich Lighting Systems, Bertramstraße 8, 59557 Lippstadt, Germany
(c) Helmholtz-Zentrum Berlin für Materialien und Energie, 14109 Berlin, Germany
(d) Ludwig-Maximilian-Universität, 81377 München, Germany
(e) Max-Planck-Institut für Festkörperforschung, 70567 Stuttgart, Germany

A lithium-ion capacitor (LIC) was studied during an extensive charge/discharge procedure. Changes in the interior three-dimensional structure were investigated by means of X-ray tomography during electrical cycling of the LIC. With increasing number of cycles we found electrolyte accumulating at the bottom of the capacitor. A clear correlation between electrolyte distribution at the bottom and performance of the LIC was determined.

Introduction

Fuel cells and batteries are among the most important components needed for future mobile and stationary energy supply [1-2]. In many cases, e.g. during (de)acceleration of automotive and railway systems, the storage systems have to withstand very high current densities. Batteries can store large amounts of electric energy, but are highly sensible to heavy current loads especially during charging cycles. Technical systems rely on a combination of high-power components, mostly capacitors or superconductors, and high-energy storage systems (batteries) to match the conflicting requirements [3-6]. Recent development of capacitors introduced lithium-ion capacitors (LIC), which can be regarded as hybrid systems, combining parts of lithium ion batteries, e.g. lithiated carbon, with typical supercapacitor components, e.g. electrolytes and porous graphite electrodes [7-9].

In recent years, tomographic and radiographic measurement techniques based on X-rays and neutrons have been successfully applied to study batteries and fuel cells [10-21]. These techniques are non-destructive and non-invasive, i.e. structural changes can be monitored without interfering with the operating conditions of the devices [22]. Neutron tomography and synchrotron X-ray tomography have been used for investigations of alkaline manganese dioxide batteries [23-25]. Furthermore, X-ray tomography was applied for structural investigations of lithium ion batteries [16, 26].

In this paper, we demonstrate the large potential of 3D X-ray imaging for the investigation of lithium-ion capacitors. The focus of the present study is on the correlation between electrolyte distribution and capacity.

Experimental Method

Tomographic Imaging

The imaging experiments were performed at Helmholtz-Zentrum Berlin using an X-ray micro-tomography (µCT) device (see Figure 1) [27]. Major components of this device are a micro-spot X-ray tube, a translation-rotation unit and a 5.4 megapixel flat panel detector with a pixel size of d=50 µm. According to the cone beam geometry generated by the X-ray source, each camera pixel images a sample area of size R, which is given by the source-object-distance (SOD), the source-detector-distance (SDD) and the detector pixel size:

$$R = \frac{SOD}{SDD} \cdot d \qquad (1)$$

SOD and SDD were set to 120 mm and 298 mm, respectively, corresponding to R=19.76 µm, which determines image resolution since the X-ray spot is much smaller. This adjustment allowed for recording a tomogram of the entire LIC battery at highest possible resolution. A complete radiographic scan comprises 1200 radiographic projections covering an angular range of 360°. The exposure time for a single radiogram was 0.5 s resulting in a total acquisition time of 1 hour and 11 minutes. A filtered back-projection algorithm was employed to reconstruct the 3D volume from the radiographic data set.
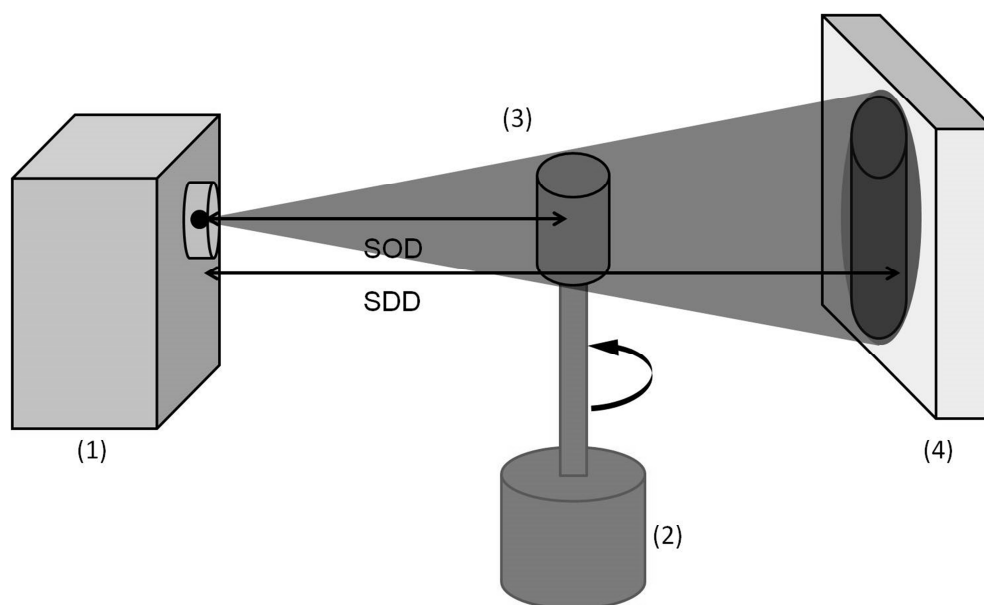
Figure 1. Schematic drawing of the setup of the µCT-measurement with the X-ray source (1), the rotation unit (2) and the fixed sample (3) and the flat panel detector (4)

<u>Electrical setup</u>

The LIC was cycled using a computer controlled voltage/current source (Yokogawa GS610). All relevant electrical data were recorded on a PC that was also used to calculate the performance data of the LIC, e.g. charged and discharged capacity, energy and efficiency.

<u>Measuring procedure</u>

Prior to cycling, a tomograph of the pristine LIC was recorded as a reference. The LIC was cycled (2.2 V <= U <= 3.8 V, $I_{const.}$= 3 A). During electrical cycling the LIC was fixed in a horizontal position. Tomograms of the charged LIC were taken after 10, 100, 500, 5000 and 10000 cycles in the upright orientation, see figure 1.

Results and discussion

A typical radiogram of the LIC is shown in Fig. 2. A cylindrical metal container is used as housing. The two current collectors are marked by arrows at the top of the capacitor (1). They extend halfway down into the interior of the capacitor. One of the collectors is made of copper (anode side), the other of aluminum (cathode side). The electrodes consist of a lithium-doped graphite anode distributed on a copper foil and a cathode, which is made from activated carbon and is applied to an aluminum foil. A separator is arranged between the two electrodes to prevent a short circuit. This assembly of foils is tightly coiled up (2) in order to efficiently utilize the space provided in the housing. The vertical lines in the radiogram displayed in figure 2 are caused by the highly absorbing Cu-foil of the anode.
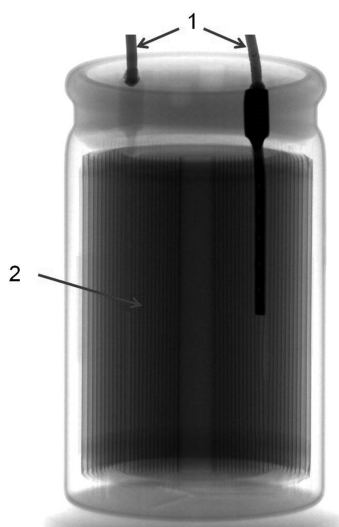
Figure 2. X-ray radiogram of the LIC under investigation. In the upper part the two current collectors (1) are shown. The bulk of the LIC consists of the coiled electrical double layer (2).

Figure 3 gives an overview of the reconstructed volume of the LIC. The tomogram was cut in different ways to provide insight into its internal structure. The vertical cross sections in figure 3(b) show the spiral electrical double layer as well as one of the embedded current

collectors. The detail in figure 3(c) displays the bottom area where the electrolyte tends to accumulate. Furthermore, a horizontal cross section is displayed in figure 3(d) showing the winding of the electrode assembly. This perspective allows for identifying delamination effects and other manufacturing irregularities, as demonstrated in the detail of figure 3(e).
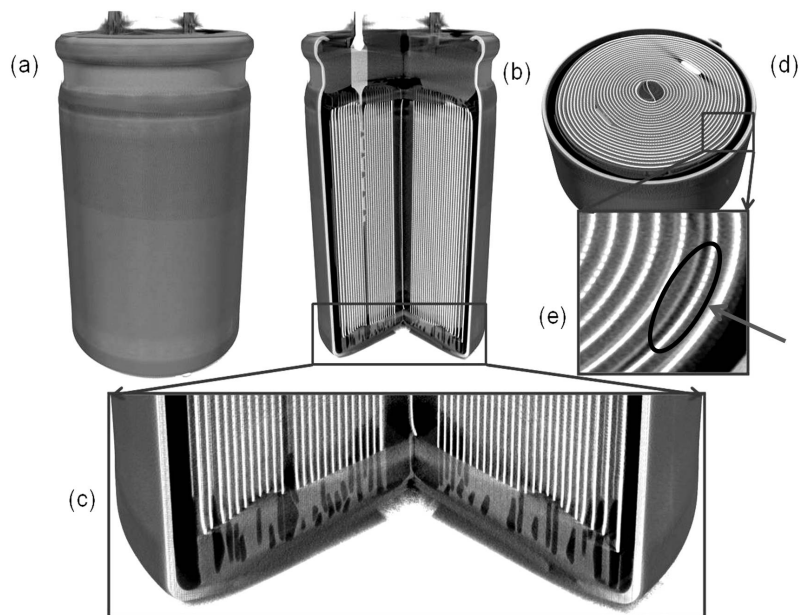
Figure 3. Overview of the interior structure of the LIC. (a) Side view of the metal container with the current collectors on top; (b) side view after virtual removal of a part of the volume; (c) enlargement of the bottom section; (d) horizontal cross section; (e) enlargement of the part of (d) where a delamination is visible.

We focus on horizontal slices selected at a height within the bottom region of the LIC in order to study the electrolyte distribution at different stages of component lifetime, i.e. for an increasing number of charge-discharge cycles. Figure 4 shows a reconstructed tomogram of the pristine LIC. Two horizontal cross sections taken from the tomogram at two different locations are shown in figures 4(b) and 4(c). The first cross section was taken at about medium height within the electrochemically active region of the LIC. The other one was taken from the bottom area, i.e. underneath the active region, were the electrolyte tends to accumulate.
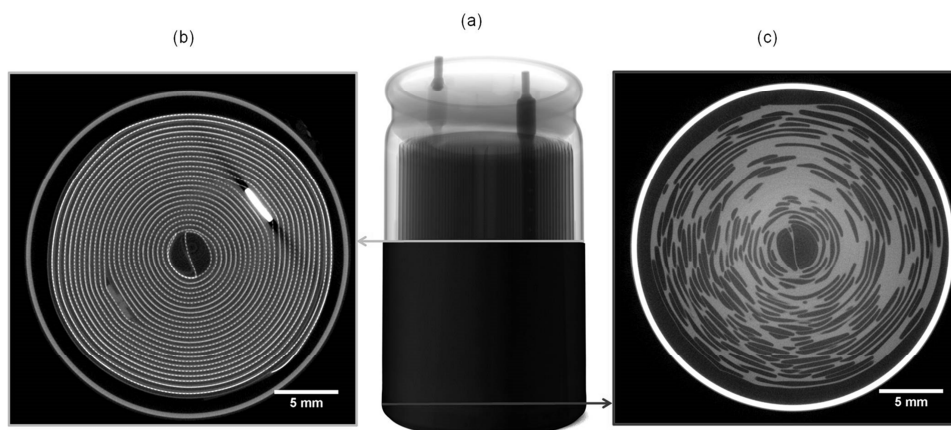
Figure 4. (a) 3D view of a pristine LIC including two horizontal cross sections through the middle (b) and the bottom (c) part of the tomogram (a). The highly absorbing components in the active region are the current collectors.

In order to analyze the electrolyte distribution in the bottom region quantitatively, the tomographic data was binarized. Figure 5 illustrates the binarization approach for a selected tomographic slice of an uncycled LIC. A region of interest (ROI) is defined that excludes the highly absorbing cell housing (see figure 5b). After this, the image data is binarized using an appropriate threshold, see figure 5c.
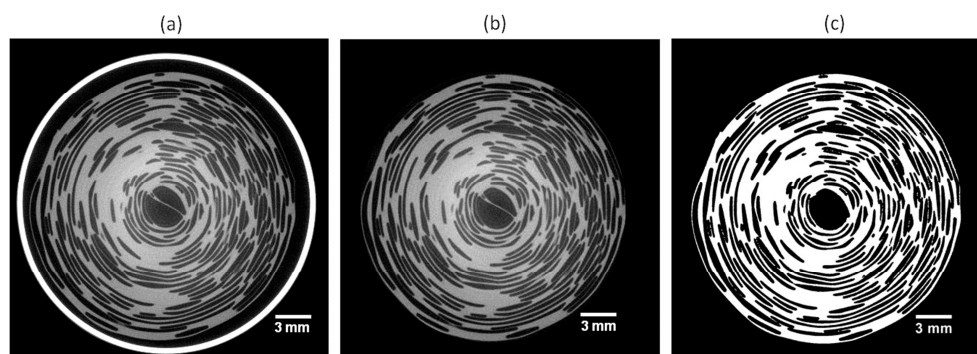
Figure 5. Basic approach to binarize the image data. (a) cross section through the bottom area; (b) region of interest without highly absorbing casing; (c) binarized cross section, using an appropriate threshold.

Figure 6 shows an image series of the cross sections from the bottom region of the LIC at cycle numbers ranging from 0 to 10000. The accumulation of electrolyte at the bottom indicates that there is a loss of electrolyte from the active coil in the LIC. The strongest increase of leaked electrolyte was found between 500 and 5000 cycles.
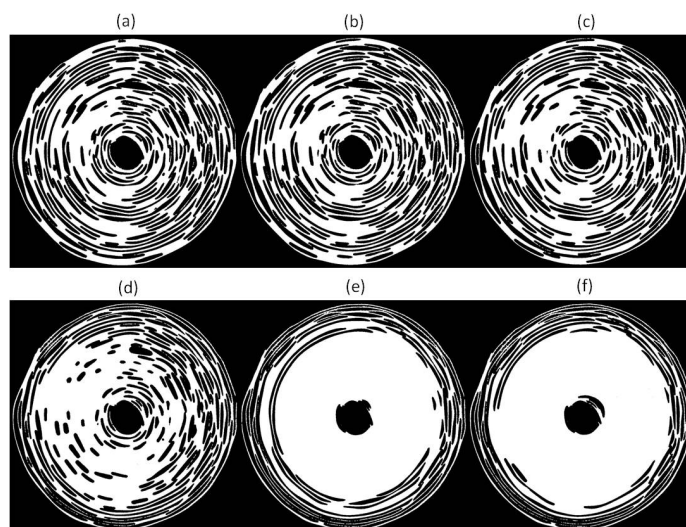
Figure 6. Binarized images of the same reconstructed slice taken after (a) 0; (b) 10; (c) 100; (d) 500; (e) 5000; (f) 10000 cycles.

Table 1 shows a summary of the binarized images. The accumulation of the leaked electrolyte after 10000 cycles increases by 20 %. During the first 100 cycles the amount of the electrolyte shows no significant increase. The effect becomes clearly visible after 500 cycles.

Table I. Quantification of the electrolyte content for increasing cycle number as derived from Fig. 6

cycle number	0	10	100	500	5000	10000
amount of electrolyte in %	52	53	54	58	70	72

This information can be correlated to the electrical performance of the LIC. In figure 7, the dependence of discharge time per cycle (fig 7a) and nominal capacity (fig 7b) on the cycling number is plotted. After 500 cycles the nominal capacity and the discharge time per cycle were decreased by about 8 %. After 5000 cycles the nominal capacity was about 70%. This corresponds to the electrolyte accumulation observed in the imaging experiments (see table 1 and figure 6). The correlation of electrical and imaging data suggests that the electrolyte distribution is closely linked to ageing mechanisms of the LIC.
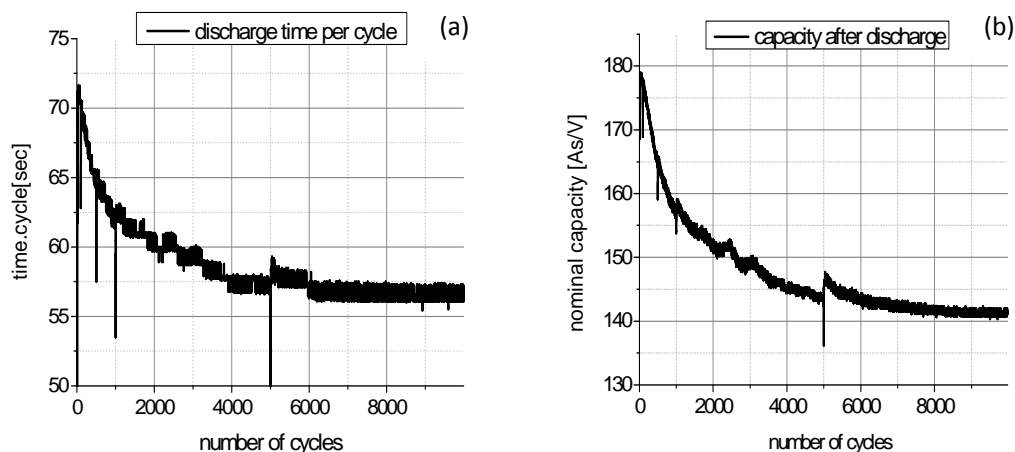
Figure 7. Discharge time (7a) and nominal capacity (7b) of the LIC after different cycling numbers; a strong decrease occurs during the first 5000 cycles, after which the nominal capacity and time per discharge cycle approaches a constant value.

Summary

It was shown that X-ray tomography is ideally suited for a non-destructive and non-invasive investigation of the electrolyte distribution in lithium-ion capacitors. We found a clear correlation between the amount of electrolyte leaked from the active coil and accumulated at the bottom of the housing and the capacity of the LIC. In future experiments, studies on the correlation of electrolyte distribution and capacitor performance will be extended to other types of capacitors.

1. D. Linden and T. B. Reddy, edited by L. D. (McGraw-Hill, New York, 2002).
2. G. Hoogers, (CRC Press LLC, Boca Raton, FL,, 2003).
3. M. Vangari, T. Pryor and L. Jiang, J. Energy Eng.-ASCE **139**, 72 (2013).
4. A. Chandra, Proc. Nat. Acad. Sci. India A **82**, 79 (2012).
5. J. Xu, H. Wu, C. Xu, H. T. Huang, L. F. Lu, G. Q. Ding, H. L. Wang, D. F. Liu, G. Z. Shen, D. D. Li and X. Y. Chen, Chemistry-a European Journal **19**, 6451 (2013).
6. Y. H. Cheng, IEEE Trans. Energy Convers. **25**, 253 (2010).
7. D. Cericola and R. Kotz, Electrochimica Acta **72**, 1 (2012).
8. K. Naoi, Fuel Cells **10**, 825 (2010).
9. A. Oukaour, B. Tala-Ighil, M. AlSakka, H. Gualous, R. Gallay and B. Boudart, Electr. Power Syst. Res. **95**, 330 (2013).
10. I. Manke, H. Markoetter, C. Totzke, N. Kardjilov, R. Grothausmann, M. Dawson, C. Hartnig, S. Haas, D. Thomas, A. Hoell, C. Genzel and J. Banhart, Adv. Eng. Mater. **13**, 712 (2011).
11. R. J. Bellows, M. Y. Lin, M. Arif, A. K. Thompson and D. Jacobson, Journal of The Electrochemical Society **146**, 1099 (1999).
12. D. S. Hussey, D. L. Jacobson, M. Arif, K. J. Coakley and D. F. Vecchia, Journal of Fuel Cell Science and Technology **7**, 021024 (2010).
13. E. H. Lehmann, P. Boillat, G. Scherrer and G. Frei, Nuclear Instruments and Methods in Physics Research Section A: Accelerators, Spectrometers, Detectors and Associated Equipment **605**, 123 (2009).

14. P. Krüger, H. Markötter, J. Haußmann, M. Klages, T. Arlt, J. Banhart, C. Hartnig, I. Manke and J. Scholta, Journal of Power Sources **196**, 5250 (2011).

15. H. Markötter, I. Manke, P. Krüger, T. Arlt, J. Haussmann, M. Klages, H. Riesemeier, C. Hartnig, J. Scholta and J. Banhart, Electrochemistry Communications **13**, 1001 (2011).

16. P. R. Shearing, L. E. Howard, P. S. Jorgensen, N. P. Brandon and S. J. Harris, Electrochemistry Communications **12**, 374 (2010).

17. M. A. Hickner, N. P. Siegel, K. S. Chen, D. S. Hussey, D. L. Jacobson and M. Arif, Journal of The Electrochemical Society **155**, B427 (2008).

18. P. Boillat, G. Frei, E. H. Lehmann, G. G. Scherer and A. Wokaun, Electrochemical and Solid-State Letters **13**, B25 (2010).

19. W. Maier, T. Arlt, C. Wannek, I. Manke, H. Riesemeier, P. Krüger, J. Scholta, W. Lehnert, J. Banhart and D. Stolten, Electrochemistry Communications **12**, 1436 (2010).

20. R. Kuhn, J. Scholta, P. Krueger, C. Hartnig, W. Lehnert, T. Arlt and I. Manke, Journal of Power Sources **196**, 5231 (2011).

21. G. V. Riley, D. S. Hussey and D. L. Jacobson, in *Battery/Energy Technology*, edited by Z. Ogumi, N. J. Dudney and S. R. Narayanan, **25**, 75 (2010).

22. N. Kardjilov, I. Manke, A. Hilger, M. Strobl and J. Banhart, Materials Today **14**, 248 (2011).

23. I. Manke, J. Banhart, A. Haibel, A. Rack, S. Zabler, N. Kardjilov, A. Hilger, A. Melzer and H. Riesemeier, Applied Physics Letters **90**, 214102 (2007).

24. A. Haibel, I. Manke, A. Melzer and J. Banhart, Journal of the Electrochemical Society **157**, A387 (2010).

25. L. Binder and K. Kordesch, Journal of Electroanalytical Chemistry **180**, 495 (1984).

26. C. Hoch, H. Schier, C. Kallfass, C. Totzke, A. Hilger and I. Manke, Micro & Nano Letters **7**, 262 (2012).

27. N. Kardjilov, A. Hilger, I. Manke, M. Strobl, M. Dawson, S. Williams and J. Banhart, Nuclear Instruments and Methods in Physics Research Section A: Accelerators, Spectrometers, Detectors and Associated Equipment **651**, 47 (2011).